

# Dynamic Tensile Characterization of a 4330-V Steel with Kolsky Bar Techniques

B. Song · B.R. Antoun · H. Jin

Received: 14 August 2012 / Accepted: 15 January 2013 / Published online: 7 June 2013  
© Society for Experimental Mechanics 2013

**Abstract** Dynamic tensile experimental techniques of high-strength alloys using a Kolsky tension bar implemented with pulse shaping and advanced analytical and diagnostic techniques have been developed. The issues that include minimizing abnormal stress peak, determining strain in specimen gage section, evaluating uniform deformation, as well as developing pulse shaping for constant strain rate and stress equilibrium have been addressed in this study to ensure valid experimental conditions and obtainment of reliable high-rate tensile stress–strain response of alloys with a Kolsky tension bar. The techniques were applied to characterize the tensile stress–strain response of a 4330-V steel at two high strain rates. Comparing these high-rate results with quasi-static data, the strain rate effect on the tensile stress–strain response of the 4330-V steel was determined. The 4330-V steel exhibits slight work-hardening behavior in tension and the tensile flow stress is significantly sensitive to strain rate.

**Keywords** Kolsky tension bar · Stress–strain response · 4330-V steel · Strain rate effect · Tensile characterization

## Introduction

Most materials exhibit some strain-rate dependency, which motivates mechanical characterization in tension over a large range of strain rates. There have been ASTM standards developed for quasi-static tensile characterization of materials. However, no standard has been developed yet for dynamic tensile characterization of materials because of immature high-rate experimental techniques. The Kolsky

bar, also widely known as split Hopkinson bar, has been accepted for dynamic characterization of materials since it was developed in 1949 [1]. The original Kolsky bar was developed in compression [1]. The Kolsky compression bar has thereafter been continuously modified and improved to precisely determine the compressive response of materials at high strain rates between  $10^2$  and  $10^4 \text{ s}^{-1}$  [2]. The first Kolsky tension bar was developed by Harding et al. [3] one decade after the first Kolsky compression bar was developed. Since then, several different versions of Kolsky tension bar have been developed by Hauser [4], Lindholm and Yeakley [5], Kawata et al. [6], Nicholas [7], Staab and Gilat [8], Nemat-Nasser [9, 10], and Brown et al. [11]. The Kolsky tension bars have been utilized to characterize cylindrical alloys [7, 12–14], sheet metals [15–18], composites [19], and polymers [11, 20] at high strain rates in tension.

In order to ensure the specimen being loaded at constant strain rates under stress equilibrium, pulse shaping technique has been developed for Kolsky compression bar experiments [21]. However, the pulse shaping technique has a limited application to current Kolsky tension bar experiments. Song et al. [22] have recently improved the current common design of Kolsky tension bar for obtaining precise high-rate response of materials in tension. In their design, a solid striker was used to impact an end cap on the gun barrel that also served as part of loading device [22]. This design enables direct application of the pulse shaping technique extensively used in Kolsky compression bar experiments, to dynamic tensile experiments.

The testing conditions in Kolsky tension bar experiments are needed to be carefully checked even though the pulse shaping is applied. As compared to Kolsky compression bar testing, the techniques used to grip specimens in Kolsky tension bar experiments are much more complicated. The complicated specimen geometry and tension bar system make it more challenging to check the testing conditions

---

B. Song (✉) · B.R. Antoun · H. Jin  
Sandia National Laboratories, Livermore, CA 94551, USA  
e-mail: bsong@sandia.gov

and to measure stress and strain precisely in the specimen. For example, the specimen in a Kolsky tension bar experiment needs to be firmly attached to the ends of incident and transmission bars, which can be either glued on or threaded into the ends of both incident and transmission bars. Threading the specimen into the bar ends has been a more practical specimen installation process. However, the imperfect thread connections between the specimen and the bar ends may result in an abnormal stress peak in the tensile stress–strain response of the material under investigation [13, 17, 18, 23]. This pseudo stress peak has been concluded to be an experimental artifact, which should be minimized [24]. Applying Teflon tape on the threads became an efficient method to minimize the amplitude of the pseudo stress peak [24].

After the pseudo peak stress is minimized, attention needs to be paid to validating the testing conditions in Kolsky tension bar experiments. As mentioned earlier, the specimen is required to deform uniformly such that the average deformation over the specimen gage length can represent any point-wise deformation on the specimen. In most cases, the uniformity of deformation is related to stress equilibration. Generally, it is easier to check stress equilibrium rather than uniformity of deformation in Kolsky bar experiments since the stress histories at both ends of the specimen are measurable [2]. The stress at the incident bar/specimen end can be calculated with the incident and reflected pulse while the stress at the specimen/transmission bar end is calculated with the transmitted pulse. Then the stress equilibrium can be evaluated by applying appropriate criteria to the stress histories at both ends of the specimen [25],

$$\Delta = 2 \left| \frac{\varepsilon_i + \varepsilon_r - \varepsilon_t}{\varepsilon_i + \varepsilon_r + \varepsilon_t} \right| < 5\% \quad (1)$$

where  $\varepsilon_i$ ,  $\varepsilon_r$ , and  $\varepsilon_t$  are incident, reflected, and transmitted pulses, respectively. Here it is assumed that both incident and transmission bars are made of the same material and have the same cross-sectional area. Equation (1) has been widely used to assess the stress equilibrium in Kolsky compression bar experiments. However, in Kolsky tension bar experiments, the reflected pulse may not be reliable because the stress wave is disturbed at the interfaces of adapters and couplers as well as threads [22]. Therefore, it challenges precise measurement of both displacement and force at the incident bar end. It would be erroneous if equation (1) is used for evaluation of stress and strain uniformity. It is thus desirable to develop a reliable method to evaluate the uniformity of deformation in Kolsky tension bar experiments.

Advanced diagnostic techniques are needed to monitor the strain field over the specimen gage length in real time, particularly under high-rate tensile loading. Digital image correlation (DIC) has recently been fast growing for full field deformation measurement during mechanical tests. The DIC technique has been applied to Kolsky tension bar

experiments [16, 26]. Compared to taking the average strain measurement from the conventional Kolsky bar analysis, the DIC technique provides full-field detailed deformation information. Gilat et al. [16] concluded that the DIC results agreed with the results from conventional Kolsky bar analysis before necking occurred. Once necking occurred, the conventional Kolsky bar analysis is no longer applicable; whereas, DIC was still able to provide useful information of the localized deformation. Other optical methods have also been developed to measure the local deformation of the Kolsky bar tensile specimen [14, 27].

Another challenge in Kolsky tension bar experiments is to quantitatively determine the specimen strain. The DIC method mentioned above may be capable of measuring the specimen deformation during dynamic tensile loading. However, it is still challenging for DIC to precisely measure very small strains, i.e., the elasticity of the specimen. Another limitation of current high-rate DIC technique is the sampling rate. In a Kolsky tensile bar test with a typical loading duration of 2–300  $\mu\text{s}$ , current DIC technique may not be able to obtain many data, due to the limitation of the speed of camera or the quantity of acquired images, to construct a precise stress–strain curve.

Conventional Kolsky bar analysis is difficult to directly calculate the specimen deformation in tension. The metallic tensile specimen for a Kolsky tension bar experiment is typically made into dumbbell shape to minimize stress concentration. However, the dumbbell shape specimen causes difficulty in determination of effective gage length. In quasi-static experiments, an extensometer is usually attached to the gage section to directly measure the average strain over the extensometer gage length. However, the extensometer is not feasible in Kolsky tension bar experiments. The specimen displacement calculated from a Kolsky tension bar experiment is an average measurement over the whole specimen length including both gage and non-gage sections. Appropriate determination of equivalent gage length or displacement over the gage section thus becomes critical to calculate the specimen strain.

In this study, we employed the improved Kolsky tension bar, described in Ref. [22], to characterize a 4330-V steel in tension at high strain rates. The 4330-V is a NiCrMoV hardened and tempered high strength alloy steel, which has exceptional low temperature impact properties. The unique impact properties have made the 4330-V steel be used in many oil, gas, and aerospace industries. Detailed experimental procedure of the Kolsky tension bar experiments is presented. A pulse shaping technique was employed to produce valid testing conditions. Determination of equivalent gage length for precise strain calculation was analyzed. High-rate digital image correlation (DIC) technique was employed in the Kolsky tension bar experiments, which enabled direct measurement of the strain field

over the gage length such that uniformity of specimen deformation over the entire loading duration was able to be checked. Resultant tensile stress–strain curves of the 4330-V steel were obtained and strain rate effect on the tensile flow stress was determined.

## Experimental Procedure

The newly designed Kolsky tension bar for high-rate tensile characterization of 4330-V steel was described in detail in Ref. [22]. Figure 1 shows the schematic of this Kolsky tension bar. The new design of the Kolsky tension bar employs the gun barrel as a part of loading component, which simplifies the application of pulse shaping. The pulse shaping techniques for Kolsky compression bar experiments have been well developed [2]. The design of Kolsky tension bar shown in Fig. 1 enables direct implementation of currently existing pulse shaping techniques for compression-bar experiments to the tension-bar experiments. In this study, an annealed C11000 copper disk with 6.35 mm in diameter and 0.25 mm in thickness was placed, as the pulse shaper, on the inside surface of the flange threaded into the end of gun barrel in the Kolsky tension bar experiments.

Figure 2 shows the mechanical drawing of the tensile 4330-V steel specimen. The specimen had a designed gage length of 6.35 mm and a diameter of 3.18 mm on gage section. The specimen was threaded into the bar ends via adapters (Fig. 1). As mentioned earlier, such complicated connection between the specimen and bar ends may distort the stress wave propagation [22], making equation (1) not applicable to evaluate the stress equilibrium and to calculate the displacement at the incident bar end in the Kolsky tension bar experiment.

Figure 3 shows the typical oscilloscope records of incident, reflected, and transmitted pulses obtained from the pulse-shaped Kolsky tension bar experiment. Due to the employment of the pulse shaper, the rise time in the incident pulse increased from the typical 10 microseconds in conventional Kolsky bar experiments to nearly 100 microseconds, providing sufficient time for the specimen to achieve stress equilibrium or uniform deformation. Again, the reflected pulse shown in Fig. 3 may not be reliable to measure the force and displacement at the incident bar end, which motivates the application of an alternative

optical method to the Kolsky tension bar experiments for uniform deformation verification.

DIC has been proven capable of full field strain measurement on the specimen during quasi-static loading. In this study, we applied the DIC technique to Kolsky tension bar experiments to evaluate the state of uniform deformation associated with stress equilibrium under dynamic loading. To avoid the delamination of DIC speckle patterns from the specimen surface during high strain rate testing, the specimen surface was first sand blasted and ultrasonically cleaned with isopropyl alcohol. A random speckle pattern was then generated by spraying black paint directly onto the cylindrical surface of the steel specimen. No white base layer was applied. A Phantom V12.1 high speed digital camera was used to photograph the specimen deformation at a speed of 83,000 frames per second (FPS). The camera was focused only on a small cross-sectional area to achieve sufficient image resolution. The whole gage section and part of non-gage section at both ends were selected as area of interest (AOI) for DIC analysis, as shown in Fig. 4.

Figure 5 shows the strain distribution along the specimen gage length based on the DIC analysis. The DIC analysis covered part of non-gage section such that the strain at both ends is smaller due to the larger cross-sectional area at non-gage section. We also attached a strain gage on the back surface of the specimen to compare with the DIC output. The DIC results are very consistent with the strain gage output, showing the 2-D DIC is satisfied to analyze the actual 3-D deformation in this case. However, the relatively small amount of data points from DIC analysis due to the limited speed of digital camera is not sufficient to construct a precise stress–strain curve. Therefore, the DIC data were not used for determination of resultant stress–strain curve. Due to the relatively short specimen gage length (6.35 mm), high elastic wave speed ( $\sim 5,000$  m/s) in the specimen material, as well as appropriate pulse shaping design, the specimen was observed to be in a state of uniform deformation very quickly, e.g., when the specimen was still under elastic deformation (Fig. 5) at  $t=12 \mu\text{s}$ . It was interesting that the specimen was then observed to undergo non-uniform deformation when  $84 < t < 108 \mu\text{s}$ . However, the non-uniformity of deformation was not significant even though the DIC images show significant discolor due to variable scales being used here. The specimen deformation then became more significantly localized at the center of the specimen

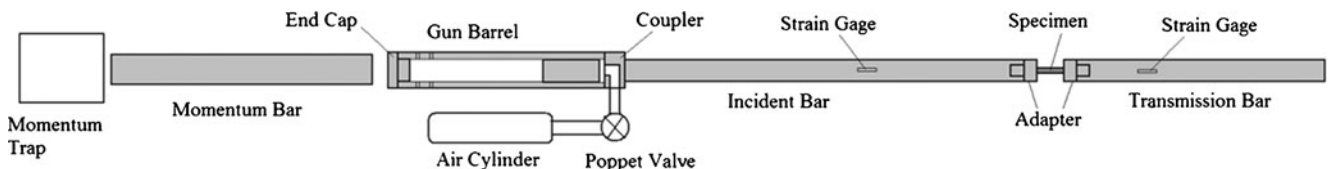
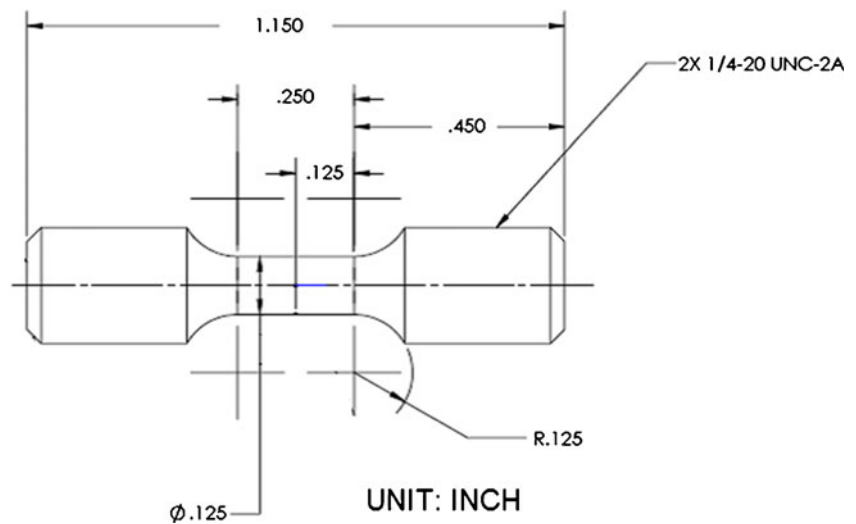


Fig. 1 Schematic of Kolsky tension bar system

**Fig. 2** Tensile specimen design

gage section and was progressively accumulated while being globally stretched. This localized plasticity may be related to the stress response at yield and in plasticity. The mechanism of this localized plasticity at high rates is still under investigation.

Figure 6 shows the stress history at the back end of the specimen, which was calculated from the transmitted signal [2],

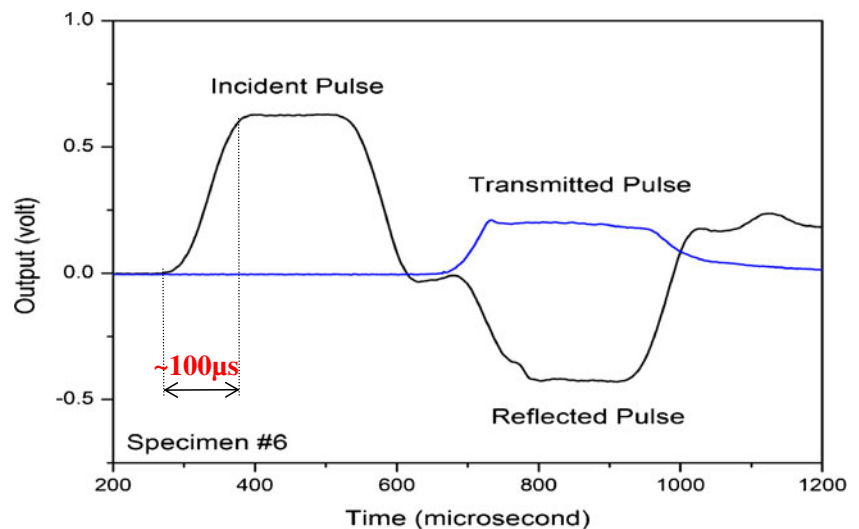
$$\sigma = \frac{A_b}{A_s} E \varepsilon_t \quad (2)$$

where  $A_b$  and  $A_s$  are cross-sectional area of the pressure bars and the specimen, respectively;  $E$  is Young's modulus of the pressure bar material. Combining Figs. 5 and 6, it is concluded that the specimen was in uniform elastic deformation. When the specimen begins to deform plastically, the deformation is localized. However, the specimen stress history shows insignificant work hardening characteristic. In this case, the stress equilibrium deviates from uniform deformation. In other words, the stress in the specimen may be equilibrated, due to insignificant work hardening behavior, but this equilibrium

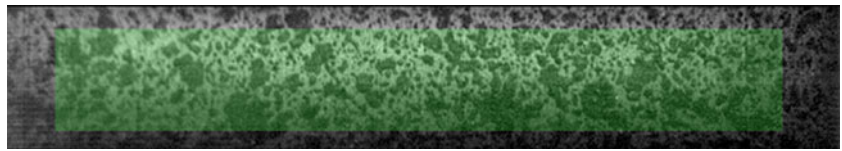
does not represent uniform deformation. Therefore, the specimen stress can still be calculated with the transmitted signal (Fig. 2), but it becomes much more challenging to determine specimen strain. Similar phenomenon has been or even more severe, observed in foam/cellular materials [28]. The mechanism of non-uniform deformation in the alloy is still under investigation. In order to estimate the high-rate stress–strain response of this material, we followed the conventional method that takes the average strain over the specimen gage length to estimate the specimen strain,

$$\varepsilon = \frac{\Delta L_s}{l_s} \quad (3)$$

where  $\Delta L_s$  is the displacement applied to the specimen gage section;  $l_s$  is the gage length of the specimen. For the design of tensile specimen shown in Fig. 2, it is difficult to directly measure the displacement over the specimen gage section. Instead, we measure the total specimen displacement that includes both gage and non-gage section displacement. Therefore, equation (3) needs to be corrected,

**Fig. 3** Typical oscilloscope record of incident, reflected, and transmitted pulses

**Fig. 4** High-rate digital image correction (DIC) over specimen gage length



$$\varepsilon = c' \frac{\Delta L_T}{l_s} = c' \frac{\Delta L_s + \Delta L}{l_s} \quad (4)$$

where  $\Delta L_T$  is the total displacement over the specimen length including both gage section ( $\Delta L_s$ ) and non-gage section ( $\Delta L$ );  $c'$  is correction coefficient.

Figure 7 illustrates the detail of one end of the non-gage section. At a certain load  $F$ , the strain distribution along the non-gage section is

$$\varepsilon(x) = \frac{F}{E_s A(x)} \quad (5)$$

where  $E_s$  is Young's modulus of the specimen material;  $A(x)$  is the cross-sectional area,

$$A(x) = \pi r(x)^2 \quad (6)$$

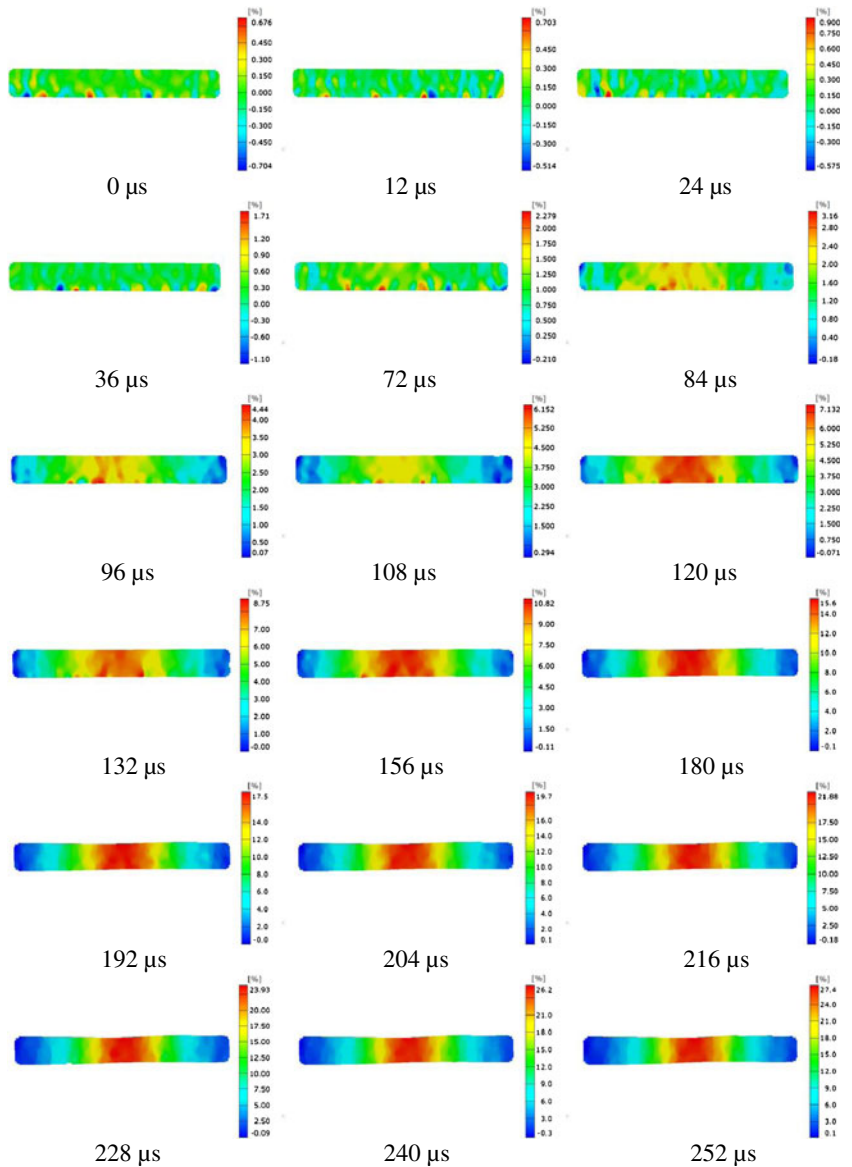
According to Fig. 8, the radius for the non-gage section is expressed as

$$r(x) = R + r_0 - \sqrt{R^2 - x^2} \quad (7)$$

where

$$r(0) = r_0 \quad (8a)$$

**Fig. 5** Specimen strain field from high-rate DIC analysis



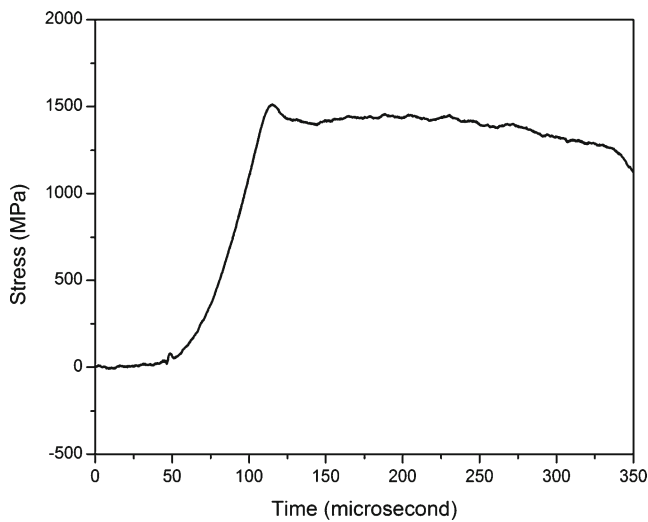


Fig. 6 Stress history in the specimen

$$r(x_0) = r_1 \tag{8b}$$

where  $r_0$  is the radius on gage section and  $r_1$  is the thread radius. The total displacement occurred on the non-gage section is

$$\Delta L = 2 \int_0^{x_0} \varepsilon(x) dx = 2 \int_0^{x_0} \frac{F}{E_s \pi (R + r_0 - \sqrt{R^2 - x^2})^2} dx \tag{9}$$

In this study,  $r_0 = 1.59 \text{ mm}$ ,  $r_1 = 3.18 \text{ mm}$ ,  $x_0 = 2.75 \text{ mm}$ . Integrating equation (9) we have

$$\Delta L = \frac{1.474F}{E_s \pi} (\text{mm}) \tag{10}$$

When the load  $F$  is not sufficiently high to yield the specimen, the gage section is responding elastically. The total displacement over the gage section is

$$\Delta l_s = l_s \varepsilon_s = \frac{F}{E_s \pi} \cdot \frac{l_s}{r_0^2} \tag{11}$$

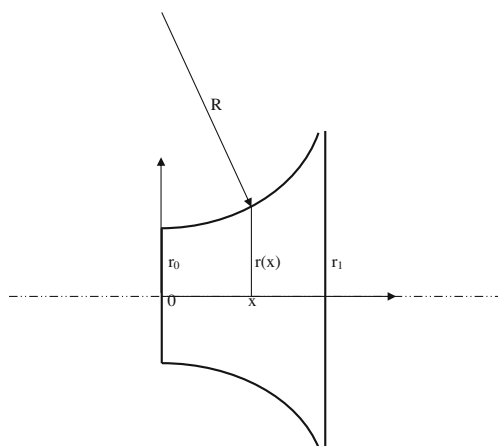


Fig. 7 Schematic of one end of the non-gage section of the tensile specimen

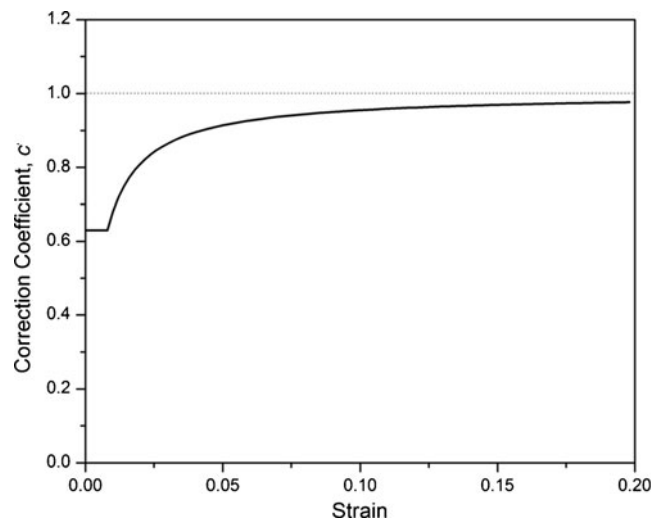


Fig. 8 Dependency of correction coefficient,  $c'$ , on specimen strain

where  $l_s = 6.35 \text{ mm}$  in this study. Therefore, the gage-section displacement is simplified as

$$\Delta l_s = l_s \varepsilon_s = \frac{2.512F}{E_s \pi} (\text{mm}) \tag{12}$$

The correction factor,  $c'$ , in equation (4) is calculated as

$$c' = \frac{\Delta l_s}{\Delta L + \Delta l_s} \tag{13}$$

It is noted that equation (13) is applicable only while the gage section is responding elastically. Since the 4330-V material exhibits insignificant work-hardening, we used the assumption of perfect plasticity to estimate the plastic strain. In this case, the gage section becomes plastic while the non-gage section still remains elastic due to its larger cross sectional area (or lower stress than yield strength). The displacement over the non-gage section is calculated with equation (10),

$$\Delta L = 1.474r_0^2 \varepsilon_y (\text{mm}) \tag{14}$$

where  $\varepsilon_y$  is yield strain. In this study, the yield strain was measured from quasi-static experiments,  $\varepsilon_y = \frac{\sigma_{0.2}}{E} = 0.8\%$ . The total displacement over the non-gage section was thus calculated,  $\Delta L = 0.03 \text{ mm}$ . The gage-section displacement is rewritten as

$$\Delta l_s = l_s \varepsilon_p \tag{15}$$

or

$$\Delta l_s = \Delta L_T - \Delta L = \Delta L_T - 0.03 (\text{mm}) \tag{16}$$

The strain over the gage section can be calculated after the total displacement over the entire specimen length,  $\Delta L_T$ , is measured,

$$\varepsilon = \frac{\Delta l_s}{l_s} = \frac{\Delta L_T - 0.03}{l_s} \tag{17}$$

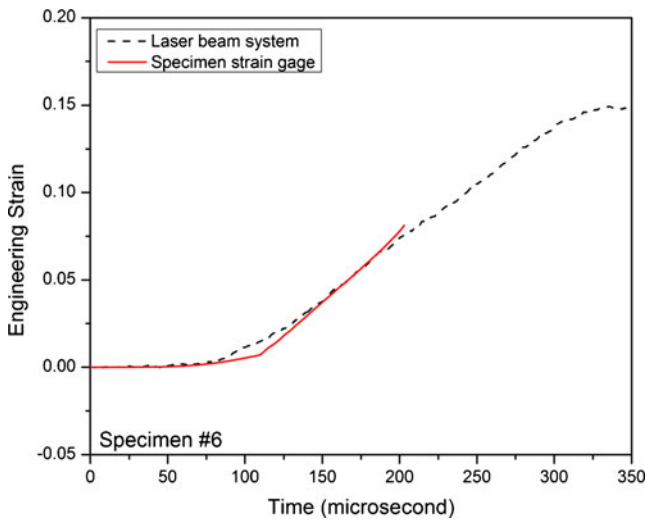


**Fig. 9** Specimen strain comparison from strain gage and laser beam measurements

Here both displacement and specimen gage length take millimeter as unit. The correction factor,  $c'$ , here depends on the total displacement,

$$c' = 1 - \frac{0.03}{\Delta L_T} \tag{18}$$

or on the plastic strain of specimen,  $\epsilon_p$ ,

$$c' = \frac{l_s \epsilon_p}{l_s \epsilon_p + 1.474 \epsilon_y r_0^2} = \frac{\epsilon_p}{\epsilon_p + 0.0047} \tag{19}$$

Figure 8 shows the dependency of correction factor,  $c'$ , on the plastic strain. The correction factor becomes larger and tends toward unity while the specimen is being stretched to very large strain. After the displacement over

the whole specimen length is measured, the specimen strain can be calculated with equation (4).

In conventional Kolsky bar experiments, the displacement applied to the specimen is calculated with the incident, reflected, and transmitted signals on the pressure bars,

$$\Delta L_T = C_b \int_0^t (\epsilon_i(t) - \epsilon_r(t) - \epsilon_t(t)) dt \tag{20}$$

where  $C_b$  is elastic wave speed in the pressure bar material. When the specimen is in stress equilibrium,

$$\epsilon_i + \epsilon_r = \epsilon_t \tag{21}$$

Equation (20) is simplified as

$$\Delta L_T = -2C_b \int_0^t \epsilon_r(t) dt \tag{22}$$

As mentioned earlier, the reflected pulse obtained from the Kolsky tension bar experiment may not be reliable to calculate the displacement. In this study, a Micro-Epsilon® optoControl 1201 laser beam system was employed to directly measure the displacement at the incident bar end. The displacement applied to the specimen can be calculated as

$$\Delta L_T = L_{laser} - C_b \int_0^t \epsilon_t(t) dt \tag{23}$$

where  $L_{laser}$  is the displacement measured with the laser beam system at the incident bar end. This laser beam system has a frequency response of 100 kHz, which is sufficient for Kolsky bar experiments. However, the dynamic resolution of 100 μm of this laser beam system is not sufficient to measure the elastic or small

**Fig. 10** Specimen strain comparison from strain gage and DIC measurements

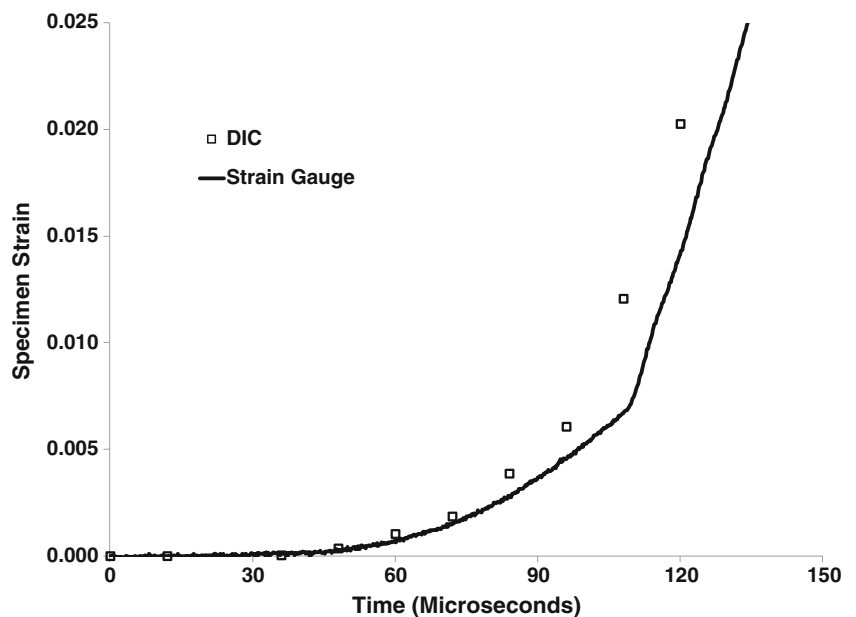
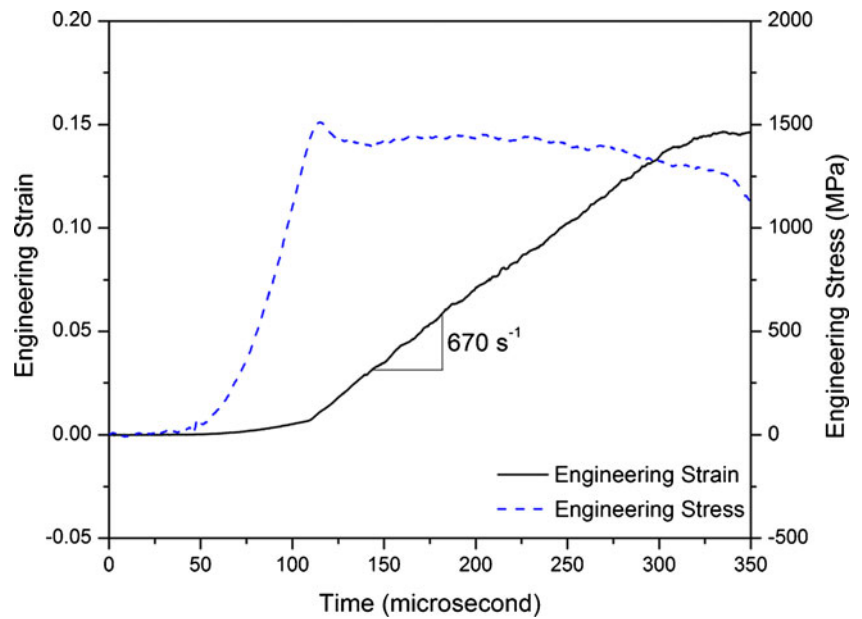


**Fig. 11** Stress and reconstructed strain histories in the specimen at  $670 \text{ s}^{-1}$



strain response of the 4330-V steel. Alternatively, we attached a strain gage on the gage section of the 4330-V steel specimen to directly measure the specimen strain up to 2 %. The strain over 2 % was measured with the laser system with appropriate correction (equations (4) and (18)),

$$\varepsilon(t) = \begin{cases} \varepsilon_g(t) & \text{when } \varepsilon \leq 2\% \\ \frac{d\Delta L_T(t)}{l_s} & \text{when } \varepsilon > 2\% \end{cases} \quad (24)$$

where  $\varepsilon_g$  is the specimen strain gage output. Differentiating equation (24) in terms of time yields the strain rate over the specimen gage length. The stress–strain curve of the specimen materials is obtained with equations (2) and (24) by eliminating the time term.

**Experimental Results**

Figure 9 shows the typical specimen strain histories which were directly measured with the specimen strain gage and calculated from the laser beam output with equations (23) and (24). It is observed that the strain measured with the laser beam system deviates from that directly measured with the strain gage on the specimen at small strains. When the strain is larger than 2 %, both measurements are consistent until the strain gage fails. We also compared the strain results from the strain gage measurement and DIC analysis at small strains, as shown in Fig. 10. The DIC results shown in Fig. 10 represent the measurement over the exact specimen strain gage area. However, the comparison results show that it is still challenging to use DIC analysis for

**Fig. 12** Engineering tensile stress–strain curves of the 4330-V steel at various quasi-static and dynamic strain rates

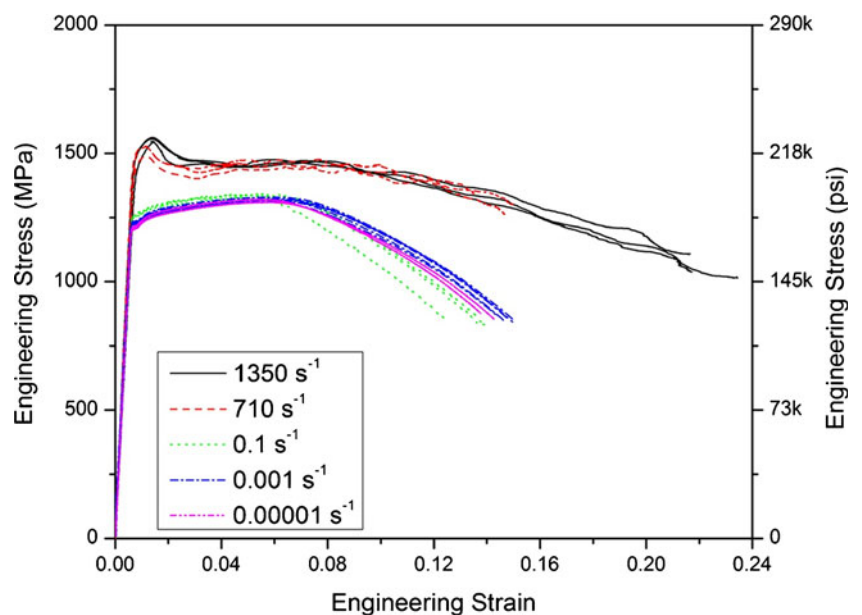
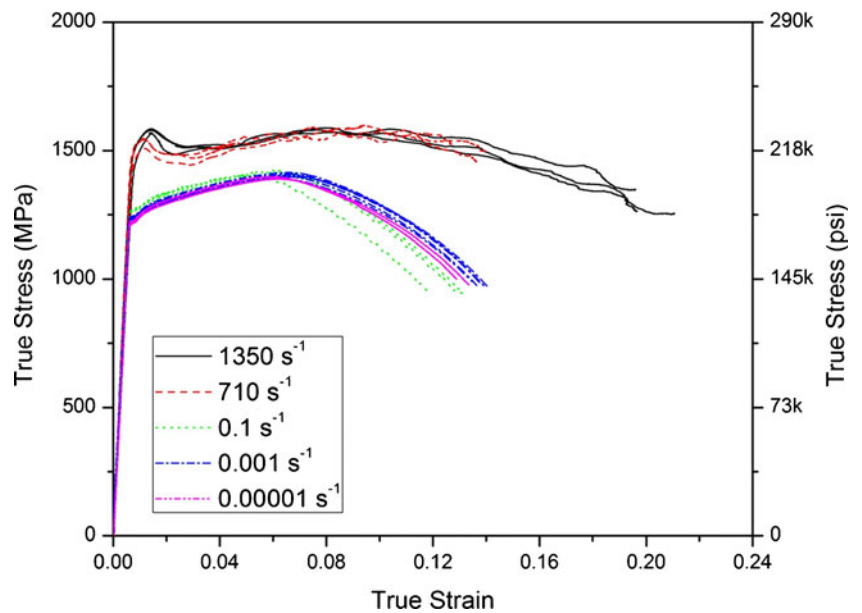




**Fig. 13** True tensile stress–strain curves of the 4330-V steel at various quasi-static and dynamic strain rates



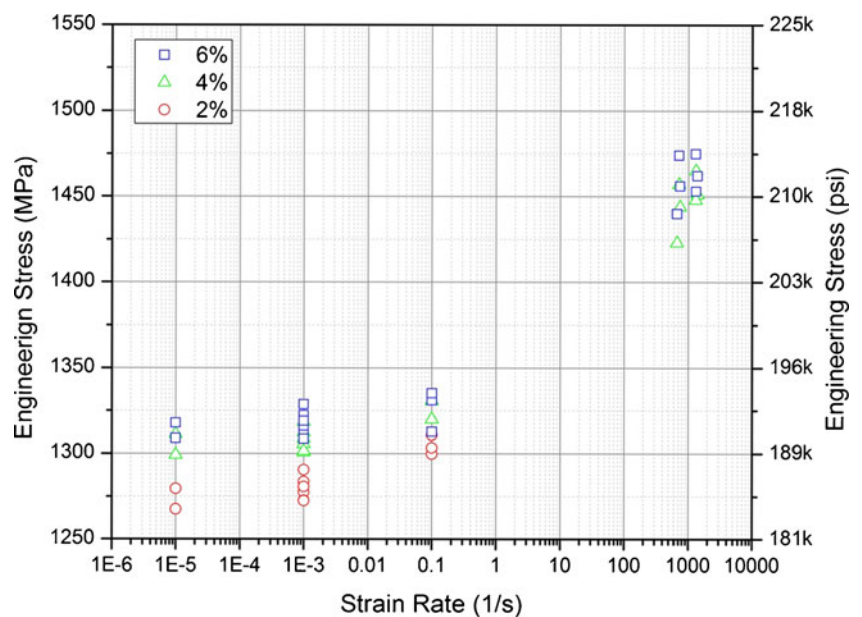
small strain measurement. The limited amount of DIC data points also discourages us using DIC data to construct the resultant stress–strain curve. Instead, we only used the DIC analysis for evaluation of deformation uniformity over the specimen gage section, as described in previous section.

We reconstructed the specimen strain history with both strain gage and laser beam measurements. The strain below 2 % was taken from the specimen strain gage measurement; whereas, the strain above 2 % was taken from the laser beam measurement. Figure 11 shows the reconstructed strain and corresponding stress history in the specimen. The nearly linear characteristic of the strain history indicates a nearly constant strain rate which was measured as  $670 \text{ s}^{-1}$ . Following the same procedure, the 4330-V steel has also been

characterized at another higher strain rate,  $1,350 \text{ s}^{-1}$ . At each dynamic strain rate, three experiments were repeated.

Figure 12 shows the engineering tensile stress–strain curves of the 4330-V steel at quasi-static ( $0.00001$ ,  $0.001$ , and  $0.1 \text{ s}^{-1}$ ) and dynamic ( $710 \pm 6 \%$  and  $1,350 \pm 4 \%$   $\text{s}^{-1}$ ) strain rates. All quasi-static and dynamic stress–strain curves exhibit similar elastic–plastic characteristics with some work hardening. We also converted the engineering stress–strain curves to true stress–strain curves which are shown in Fig. 13. The true stress–strain curves show more significant work hardening behavior. Since the tensile specimen was observed in visual necking when  $t=204$  microseconds corresponding an engineering strain of 8 % (or a true strain of 7.7 %) (Fig. 5), the stress–strain curves beyond this strain may not be reliable.

**Fig. 14** Strain rate effect on tensile flow stress of the 4330-V steel



Interpretation of stress–strain response in post-necking stage has been discussed in literature [12, 14, 23, 26].

Both Figs. 12 and 13 show that the flow stress is significantly dependent on the strain rate. Figure 14 shows detailed strain-rate effect on the tensile flow stress in engineering measurement. At a certain strain, the tensile flow stress increased nonlinearly with increasing logarithm of strain rate. The rate sensitivity at dynamic strain rates is observed more significant than at quasi-static strain rates, which has been observed in many steel alloys [7]. The mechanism might be due to thermal activation at high strain rates [23]. It is noted that the high-rate data at 2 % strain were not taken into Fig. 14 to study the strain rate effect because of small-amplitude pseudo stress peak in the dynamic tensile stress–strain response, as shown in Fig. 12. Remedies introduced in our earlier work [24] seem incapable of fully eliminating the pseudo stress peak. The tensile specimen was not sufficiently tightened into the bar ends because extra tightening load during specimen installation may subject the specimen to additional torque that results in damage in the specimen before dynamic tensile load. In order to fully eliminate the pseudo stress peak, further efforts are needed.

## Conclusions

We employed a newly developed Kolsky tension bar to characterize 4330-V steel at high strain rates. The pulse shaping technique was applied to the Kolsky tension bar experiments to validate the testing conditions. High-rate DIC technique has been employed on the Kolsky tension bar to verify the uniform deformation in the tensile specimen. Equivalent displacement over the specimen gage section was analyzed and corrected from the measured displacement over the entire specimen length including both gage and non-gage sections. The entire specimen displacement was directly measured with a high-frequency-response laser system for calculating the specimen strain over 2 %. A strain gage was attached to the specimen gage section for direct measurement of specimen strain below 2 %. The pseudo stress peak measured in the Kolsky tension bar experiments has been addressed in previous work such that the intrinsic stress response of the specimen is able to be measured. The dynamic tensile stress–strain response of the 4330-V steel was obtained from the Kolsky tension bar techniques. The 4330-V steel exhibits typical elastic–plastic behavior with slight hardening under both quasi-static and dynamic tensile loading. The yield strength and tensile flow stress are significantly strain-rate dependent from quasi-static to dynamic loading.

**Acknowledgments** The authors would like to thank Dr. Wei-Yang Lu for the valuable discussion about this work. Sandia National Laboratories is a multi-program laboratory managed and operated by Sandia Corporation, a wholly owned subsidiary of Lockheed Martin Corporation, for the U.S. Department of Energy's National Nuclear Security Administration under contract DE-AC04-94AL85000.

## References

1. Kolsky H (1949) An investigation of the mechanical properties of materials at very high rates of loading. *Proc Phys Soc Lond B*62:676–700
2. Chen W, Song B (2011) *Split Hopkinson (Kolsky) Bar: Design, Testing and Applications*. Springer, New York
3. Harding J, Wood EO, Campbell JD (1960) Tensile testing of materials at impact rates of strain. *J Mech Eng Sci* 2:88–96
4. Hauser FE (1966) Techniques for measuring stress–strain relations at high strain rates. *Exp Mech* 6:395–402
5. Lindholm US, Yeakley LM (1968) High strain rate testing: tension and compression. *Exp Mech* 8:1–9
6. Kawata K, Hashimoto S, Kurokawa K, Kanayama N (1979) A New Testing Method for the Characterization of Materials in High-Velocity Tension. In: Harding J (ed) *Mechanical Properties at High Rates of Strain*, *Inst. Phys. Conf. Ser.* 47:71–80, Oxford
7. Nicholas T (1981) Tensile testing of materials at high rates of strain. *Exp Mech* 21:177–188
8. Staab GH, Gilat A (1991) A direct-tension split Hopkinson Bar for high strain-rate testing. *Exp Mech* 31:232–235
9. Nemat-Nasser S (2000) *Introduction to High Strain Rate Testing*, vol 8, ASM handbook. Mechanical Testing and Evaluation, Materials Park, pp 427–446
10. Nemat-Nasser S, Isaacs JB, Starrett JE (1991) Hopkinson techniques for dynamic recovery experiments. *Proc Roy Soc London* 435:371–391
11. Brown EN, Rae PJ, Gray GT (2006) The influence of temperature and strain rate on the tensile and compression constitutive response of four fluoropolymers. *J Phys IV* 134:935–940
12. Rajendran AM, Bless SJ (1986) Determination of tensile flow stress beyond necking at very high strain rate. *Exp Mech* 26:319–323
13. Borvik T, Hopperstad OS, Dey S, Pizzinato EV, Langseth M, Albertini C (2005) Strength and ductility of weldox 460 E steel at high strain rates, elevated temperatures and various stress triaxialities. *Eng Fract Mech* 72:1071–1087
14. Arthington MR, Siviour CR, Petrinic N (2012) Improved materials characterisation through the application of geometry reconstruction to quasi-static and high-strain-rate tension tests. *Int J Impact Eng* 46:86–96
15. Curtze S, Kuokkala V-T, Hokka M, Peura P (2009) Deformation behavior of TRIP and DP steels in tension at different temperatures over a wide range of strain rates. *Mater Sci Eng A*507:124–131
16. Gilat A, Schmidt TE, Walker AL (2009) Full field strain measurement in compression and tensile split Hopkinson Bar experiments. *Exp Mech* 49:291–302
17. Rusinek A, Klepaczko JR (2003) Impact tension of sheet metals – effect of initial specimen length. *J Phys IV France* 110:329–334
18. Kuroda M, Uenishi A, Yoshida H, Igarashi A (2006) Ductility of interstitial-free steel under high strain rate tension: experiments and macroscopic modeling with a physically-based consideration. *Int J Solids Struct* 43:4465–4483
19. Lee D, Tippur HV, Jensen BJ, Bogert PB (2011) Tensile and fracture characterization of PETI-5 and IM7/PETI-5 graphite/epoxy composites under quasi-static and dynamic loading conditions. *Trans ASME J Eng Mater Tech* 133:021015, 11 pp

20. Nie X, Song B, Ge Y, Chen W, Weerasooriya T (2009) A split Hopkinson tension bar for extra-soft specimens. *Exp Mech* 49:451–458
21. Frew DJ, Forrestal MJ, Chen W (2005) Pulse shaping techniques for testing elastic–plastic materials with a split Hopkinson pressure Bar. *Exp Mech* 45:186–195
22. Song B, Antoun BR, Connelly K, Korellis J, Lu W-Y (2011) Improved Kolsky tension bar for high-rate tensile characterization of materials. *Meas Sci Technol* 22:045704
23. Rusinek A, Zaera R, Klepaczko JR, Cheriguene R (2005) Analysis of inertia and scale effects on dynamic neck formation during tension of sheet steel. *Acta Mater* 53:5387–5400
24. Song B, Antoun BR (2012) Pseudo stress response in kolsky tension bar experiments. *Exp Mech* 52:525–528
25. Ravichandran G, Subhash G (1994) Critical appraisal of limiting strain rates for compression testing of ceramics in a split Hopkinson Pressure Bar. *J Am Ceram Soc* 77:263–267
26. Tarigopula V, Hopperstad OS, Langseth M, Clausen AH, Hild F (2008) A study of localisation in dual-phase high-strength steels under dynamic loading using digital image correlation and FE analysis. *Int J Solids Struct* 45:601–619
27. Li Y, Ramesh KT (2007) An optical technique for measurement of material properties in the tension Kolsky bar. *Int J Impact Eng* 34:784–798
28. Song B, Forrestal MJ, Chen W (2006) Dynamic and quasi-static propagation of compaction waves in a Low-density epoxy foam. *Exp Mech* 46:127–136